Diffraction-assisted extreme ultraviolet proximity lithography for fabrication of nanophotonic arrays

Serhiy Danylyuk,[a] Hyun-su Kim, Sascha Brose, Carsten Dittberner, and Peter Loosen
Chair for the Technology of Optical Systems, RWTH Aachen University and JARA—Fundamentals of Future Information Technology, Steinbachstrasse 15, 52074 Aachen, Germany

Thomas Taubner
Institute of Physics (IA) and JARA—Fundamentals of Future Information Technologies RWTH Aachen University, 52056 Aachen, Germany

Klaus Bergmann
Fraunhofer Institute for Laser Technology, Steinbachstrasse 15, 52074 Aachen, Germany

Larissa Juschkin
Institute of Physics, EUV Sources and Applications and JARA—Fundamentals of Future Information Technologies RWTH Aachen University, 52056 Aachen, Germany

(Received 24 August 2012; accepted 10 January 2013; published 25 January 2013)

In this article, the possibilities and limitations of proximity lithography with extreme ultraviolet (EUV) radiation are explored theoretically and experimentally. Utilizing partially coherent EUV radiation with a wavelength of 10.88 nm from a Xe/Ar discharge plasma EUV source, proximity patterning of various nanoantenna arrays has been performed. The experimental results are compared with the results of numerical scalar diffraction simulations, and it is shown that proximity printing in the Fresnel diffraction mode can enable production of high-resolution features even with lower resolution masks, successfully demonstrating sub-30 nm edge resolution in the resist. The potential of the method is explored by simulation of the patterning through circular and triangular apertures as well as through bowtie antenna patterns, with the results suggesting that precise control of the proximity gap and the exposure dose together with simulation-supported mask design optimizations may allow for a wide variety of high-resolution structures to be printed through relatively simple transmission masks. The method is especially suited for high-performance manufacturing of submicrometer sized nanophotonic arrays. © *2013 American Vacuum Society*. [http://dx.doi.org/10.1116/1.4789445]

I. INTRODUCTION

There are several types of lithographic technologies that can be used as an alternative to conventional projection lithography, such as nanoimprint lithography (NIL), electron beam lithography (EBL), interference lithography, or directed self-assembly. At the end of the 20th century, one of the most promising alternatives was x-ray proximity lithography, using wavelengths around 1 nm.[1–3] With this short wavelength, the influence of the diffraction limit on the resolution is negligible, and high-resolution patterns are possible, though further reduction of the wavelength was found to be ineffective due to increased photoelectron blur in the photoresist.[3–5] Unfortunately, with this method no demagnification is possible, and the mask-to-wafer distance should be kept at the submicrometer level in order to achieve sub-30 nm resolution. Due to these strong challenges and the rapid development of immersion lithography, this technology has not progressed past the preproduction state; however, in the last decade, it was shown[6–8] that it is possible to improve resolution of the proximity printing utilizing Fresnel diffraction of the short wavelength radiation on the nanostructures. This technique achieves sub-30 nm-resolution with a mask-to-wafer gap reaching 30 μm, which is much more realistic to maintain in an industrial environment.[1] In this work, we will investigate the possibility and resolution limits of such Fresnel diffraction-assisted proximity printing with extreme ultraviolet (EUV) radiation of 10.9 nm wavelength using a laboratory EUV radiation source.

In proximity lithography, the achievable minimum feature size can be expressed as the line width, $w = b\sqrt{g\lambda}$, where b stands for a process dependent parameter on the order of unity, g stands for the proximity gap between the mask and wafer, and λ is the wavelength of radiation.[9] With an 11 nm wavelength, the achievable line width with classical proximity lithography is limited to ~100 nm with a 2 μm proximity gap; however, this limitation describes a blur caused by a classical long-range Fraunhofer diffraction from the mask and, therefore, not necessarily will be a suitable approach when considering the results of the interaction of EUV radiation with submicrometer sized mask features. For a fixed mask-to-wafer gap, g, there is a set of structure sizes, a, for which the Fresnel number, $N_F = \frac{a^2}{g\lambda}$, will be equal or larger than unity and thereby, enabling the Fresnel diffraction mode, which may allow for the production of higher-resolution features by the proximity printing at a suitable proximity gap. For EUV proximity printing, a suitable set of test structures for this method are optical nanoantennas,[10–12] which can locally enhance incident electromagnetic fields and, thus, are of great interest for a variety of applications

[a]Electronic mail: serhiy.danylyuk@tos.rwth-aachen.de

such as surface-enhanced Raman spectroscopy (SERS)[13] or surface enhanced infrared spectroscopy (SEIRS),[14,15] biosensors,[16] optical storage,[17] nanolithography,[18,19] and high-harmonic generation.[20] Since we are primarily interested in antennas for SEIRS, the single antenna size is between 250 nm and several micrometers; nevertheless, the resolution requirements are in the nanometer range due to the critical importance of the edge quality and the requirement to create nanoscale distances between the antenna electrodes to achieve even higher field enhancement.[21] Currently, such antenna arrays are mostly made by state-of-the-art EBL, which limits their industrial exploitation. On the other hand, a relatively simple setup for EUV proximity lithography with a small-scale laboratory source can enable high-volume manufacturing of high-quality nanophotonic structures.

The throughput of the technique is similar to that of x-ray proximity lithography and is limited mainly by the area of the mask and the brightness of the source. Due to the much simpler optical setup, it is not necessary to use expensive multilayer coated masks, as is true in the case of large-scale EUV lithography at 13.5 nm, which increases the yield and lowers the cost of mask manufacturing. Additionally, there is no need to put an expensive multilayer mirror in the vicinity of the EUV source, which reduces the sensitivity to contamination. Also, instead of a tin-based EUV source optimized for 13.5 nm radiation, a low-debris gas-based EUV source can be utilized. Moreover, radiation intensity losses in the optical system are much lower, which allows for efficient utilization of the EUV output of the source and decreases the requirements on the source's brightness.

II. EXPERIMENT SETUP

In this study, EUV proximity lithography utilizes a high power gas discharge-produced plasma (DPP) source developed at the Fraunhofer Institute for Laser Technology in Aachen[22,23] [Fig. 1(a)]. Such sources normally have a broadband emission spectrum in the EUV range since radiation is produced by transitions between the excited states of highly ionized heavy atoms, such as xenon or tin. However, by optimizing the gas composition of the plasma and using suitable band-pass filters, it is possible to obtain a radiation spectrum with the dominating maximum wavelength at 10.88 nm and with a bandwidth of around 3.2%.[24] The diameter of the pinch varies from 150 to 350 μm depending on the gas mixture and discharge parameters.

The laboratory setup for the EUV proximity lithography used for this study can illuminate 2 in. wafers with a single exposure field size up to 4 mm^2 [Figs. 1(a) and 1(b)].[25] The system utilizes high-precision linear positioners and a set of three capacitive sensors to control and determine the distance and tilt between the mask and the photoresist-coated silicon wafer down to tens of nanometers. Depending on the mask design and the desired structure type, negative (XR1541 [hydrogen silsesquioxane][26]) or positive [PMMA [poly(methyl methacrylate)], ZEP520A-7 (Ref. 27)] resists were used as a photoactive medium.

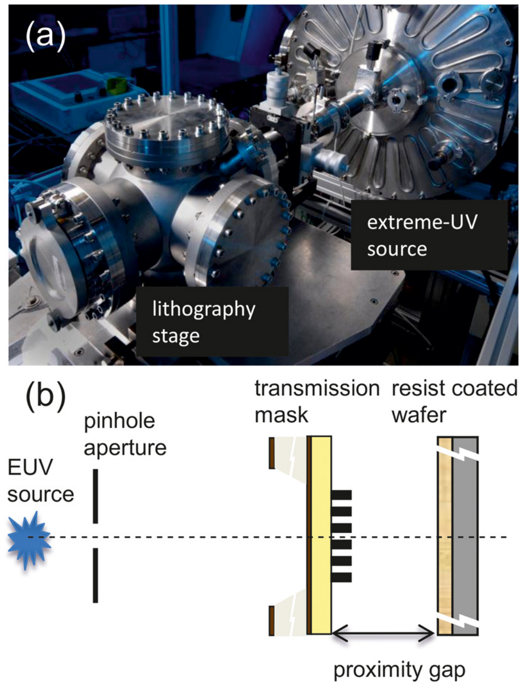

FIG. 1. (Color online) Photo (a) and scheme (b) of the experimental setup for EUV proximity lithography used in this study.

The radiation from a partially coherent source (Gaussian intensity distribution, full width at half maximum is 250 +/− 50 μm) passes through an aperture and irradiates the mask with the maximal divergence angle, $\alpha = 0.0012$ rad, given by the size of the mask (2×2 mm^2) and the distance to the source (1.67 m). The corresponding pattern-shift error, d, is equal to $d = g\tan\alpha$.[28] With the mask-to-wafer gap around 10 μm, the pattern-shift error of the system is equal to 18 nm, providing the practical resolution limit for this geometry. Reduction of the maximal divergence angle by spatial filtering or bringing the mask closer to the wafer will decrease the pattern shift error further, enabling structuring with a sub-20 nm pitch.

To support investigation at this wavelength, a novel type of transmission mask has been developed based on free-standing niobium membranes instead of the conventional Si_3N_4 supported masks. Niobium is known for its mechanical stability[29] and has a high transparency (~65% at 100 nm thickness) at the used wavelength, in contrast to highly absorbing Si_3N_4.[30] The cross-section of the transmission mask can be seen in Fig. 2. The layer system consists of the thin Nb support membrane and the structured Ni absorber layer, with the niobium simultaneously also used as a built-in filter for unwanted radiation above 16 nm. This technology can be used to produce not only masks for proximity printing but also for ultra-high-resolution interference lithography. Further details on the mask technology can be found elsewhere.[25]

For this work, a transmission mask with various popular nanophotonic antenna designs was produced. The nickel thickness of around 80 nm absorbs 98% of incoming radiation at this wavelength, allowing for excellent contrast and large process windows for processing.

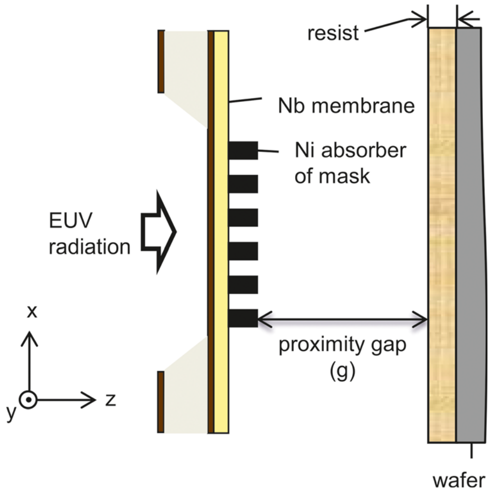

FIG. 2. (Color online) Scheme of the lithography front-end, including a transmission mask and a resist coated wafer. The coordinate system and the relevant values are defined.

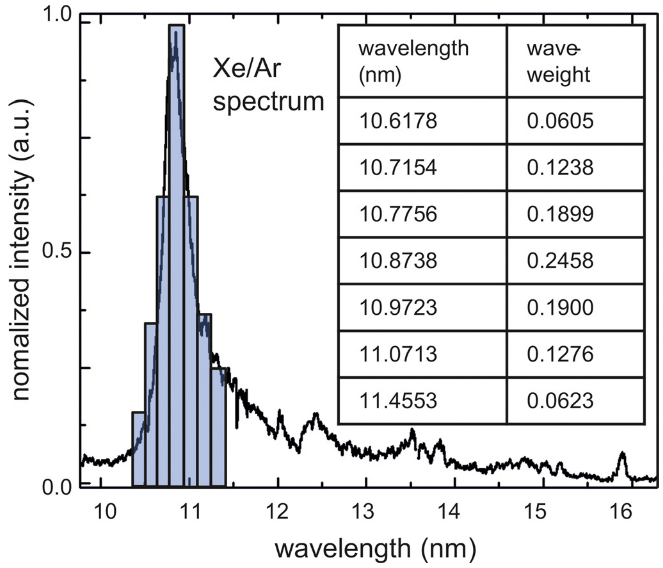

FIG. 3. (Color online) Measured emission spectrum of the DPP source with a Xe/Ar gas mixture. The set of wavelengths chosen for the simulation is shown with bars. The wavelength and relative intensity of each wavelength (waveweights) are written in the inset to the figure.

III. MODELING

Accurate simulation of the near-field diffraction is extremely important for understanding the limitations of EUV proximity lithography, and scalar simulation can be performed with the help of Fresnel–Kirchhoff (FK) diffraction or Rayleigh–Sommerfeld (RS) diffraction integrals. In our setup, where the angles of incidence and diffraction are small, those diffraction formulae give essentially the same results.[31] For the simulations, we employed the lithography simulation software developed by the Fraunhofer IISB.[32] Here we have used the RS integral of the first kind (RS I) since it was shown to produce more stable results.[32]

When the incident field is described by a spherical wave, $U = U_0 e^{ikr}/r$, the Rayleigh–Sommerfeld I approximation is expressed as

$$U_{RSI} \approx \frac{iU_0}{\lambda} \int\int \frac{e^{ik(r+r')}}{rr'} \cos(n, r) dA, \tag{1}$$

where λ is the wavelength, U_0 is the amplitude of the incident field, $k = 2\lambda/\pi$ is a wavenumber, r is the distance of the element of aperture from the observation point, r' is the distance of the element of aperture from the primary source, $\cos(n,r)$ is a diffraction angle, and A is the area of the aperture.[31] This scalar approximation is applicable when the wavelength is much smaller than both the proximity gap and the aperture size; thus, the EUV wavelength is short enough for this approximation to work with nanoantenna structures with sizes above several hundreds of nanometers and a proximity gap of several micrometers.

The broadband spectrum of the radiation and its angular divergence are implemented in the simulation where the broadband illumination is taken into account by selecting a set of wavelengths around the main peak of the spectrum and summing the different intensities generated by each wavelength. Since the radiation bandwidth of the Xe/Ar plasma source is only 3.2% (Ref. 24), the results are qualitatively very similar to the simulation performed with a single 10.88 nm wave, with only minor intensity changes visible. The seven wavelengths around 10.88 nm chosen for the simulation are shown in Fig. 3.

It is known that Fresnel diffraction patterns produced by simple round[33] and triangular[34] apertures can become rather complex. For example, in the well-studied Fresnel diffraction on a round aperture, a set of concentric rings can be observed with the number of rings depending upon an observation position.[33] In Figs. 4(a)–4(d), the results of the numerical simulation of such a diffraction are presented. Here the intensity profiles produced by the round aperture with a diameter of 1.6 μm [Fig. 4(a)] are studied as a function of the proximity gap. As expected from the analytical modeling

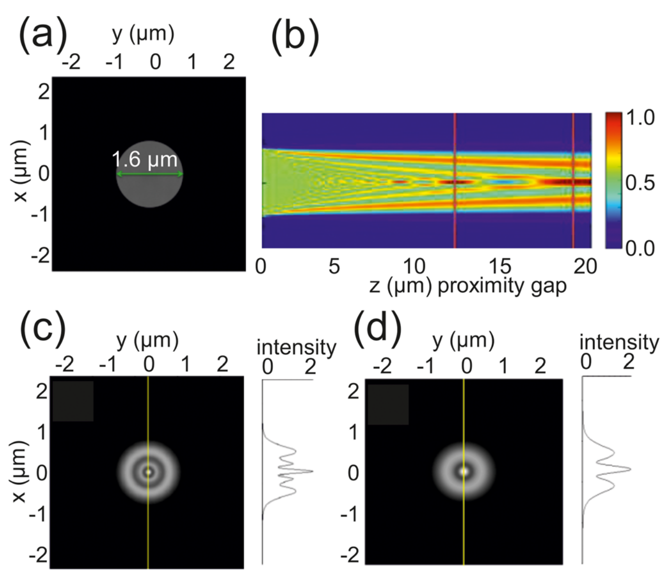

FIG. 4. (Color online) Design of the circular aperture (a) and corresponding light propagation along the z-axis (b), as well as aerial images of intensity at 12 μm (c) and 19 μm (d) proximity gaps.

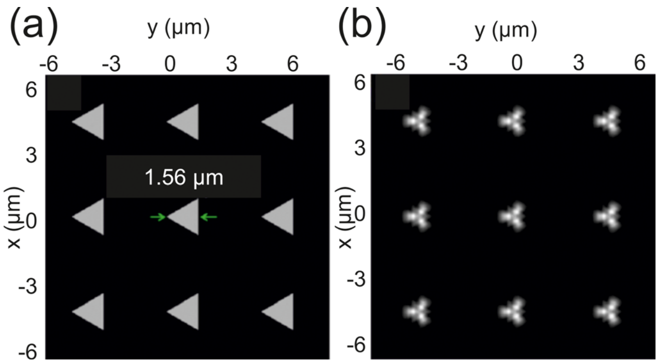

FIG. 5. (Color online) Design of the triangular aperture array (a) and the related intensity distribution behind the aperture with a 15 μm proximity gap (b).

of the diffraction, the change in the Fresnel number manifests itself in the number of visible rings (zones).

The diffraction from the triangular aperture is more complex. At a distance of 15 μm, the diffraction from an aperture of the length 1.56 μm [Fig. 5(a)] is transformed into a set of three small stabs pointing to the middle of the triangle with sub-100 nm distance between them [Fig. 5(b)].

The simulations clearly demonstrate the potential of the method to create complex nanophotonic structures of novel designs. By tuning the exposure time and modifying the proximity gap, structures of different shapes with a resolution down to sub-100 nm can be produced.

IV. RESULTS AND DISCUSSION

A. Exposure results

The experimental results of the EUV exposure through the circle and triangle apertures are shown in Fig. 6 using atomic force microscope (AFM) images after exposure and development, and inset with the corresponding simulated aerial image.

Figure 6 shows AFM images of negative high-resolution HSQ resist of 40 nm-thickness exposed through arrays of circular [Fig. 6(a)] and triangular [Fig. 6(b)] apertures at a 15 μm distance. Excellent agreement with the calculated aerial image is observed.

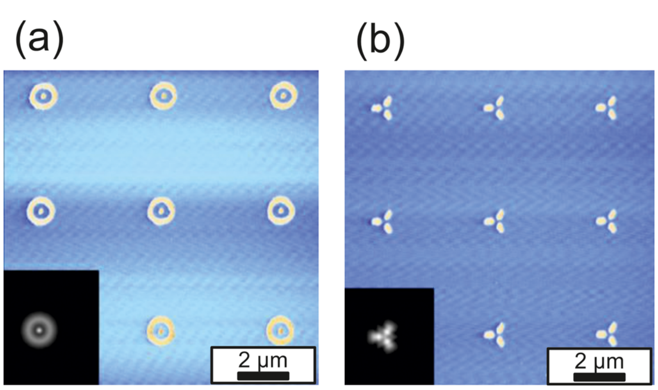

FIG. 6. (Color online) AFM images of the resists with 40 nm thickness exposed by EUV proximity lithography for circular (a) and triangular (b) apertures with a 15 μm proximity gap. Overlay images show the respective aerial images obtained from simulations.

It is also worth mentioning that the HSQ resist has demonstrated rather high contrast at this wavelength, producing structures with an edge resolution of 28 nm (measured as a change from 10 to 90% of the height of the structures). This high contrast together with the ability to tune the distance between the obtained nanophotonic antennae by changing the exposure time can allow one to obtain novel types of nanophotonic resonators. For example, the exposure through an array of simple triangle apertures at a suitable proximity gap created a set of three-antennae structures with the distance between single antennae as small as 100 nm [Fig. 6(b)].

Good correlation between the scalar diffraction simulations and experiments confirms that Fresnel diffraction is the main governing process in the EUV proximity lithography of micrometer sized structures.

Overall, the possibility to change the aerial image dramatically and controllably just by changing the proximity gap, together with the ability to fine tune the exposed resist area by variation of the exposure time, provides a very high degree of flexibility for the exposures. In combination with the developed simulation capabilities, this should enable fast and efficient design of suitable transmission masks for a wide range of interesting nanophotonic structures, including ring-disk cavities[35] or other more complex Fano-resonant antennas.[36] By controlling the gap distance with at least micrometer precision, one can, therefore, achieve reliable noncontact patterning of different structures with nanoscale resolution.

B. Optical proximity correction

The diffraction-assisted EUV lithography can also be applied to enable the high-throughput and high-quality production of traditional nanophotonic structures, such as bowties. A bowtie is one of the most popular structures in nanophotonics because of its optical properties of efficient radiation coupling and high field enhancement between the electrodes.[18–21] In this study, a mask with triangular shape apertures of 1.2 μm height, 44° opening angle, and 30 nm intertriangle distance was simulated [Fig. 7(a)]. The resulting distance between the triangles in the aerial image is strongly dependent upon the proximity gap between a mask and a wafer, and Fig. 7(b) shows the resulting aerial image (in the x–y plane) with a 5 μm proximity gap (z-axis).

To achieve a sub-100 nm distance between bowtie electrodes with this traditional mask design, the gap between the mask and wafer should be maintained at a submicrometer level, which may present a serious technological challenge. At a 5 μm mask-to-wafer gap, the minimum achievable distance between electrodes is only 450 nm at a fixed level of intensity $I = I_0/2$, where I_0 is the incoming intensity.

However, with EUV proximity printing, traditional techniques of optical proximity correction (OPC) can be used to correct and improve the image. The developed Fresnel diffraction simulation routines can be used to implement an iterative modification of the mask design, realizing a significant reduction of the achievable distance between the

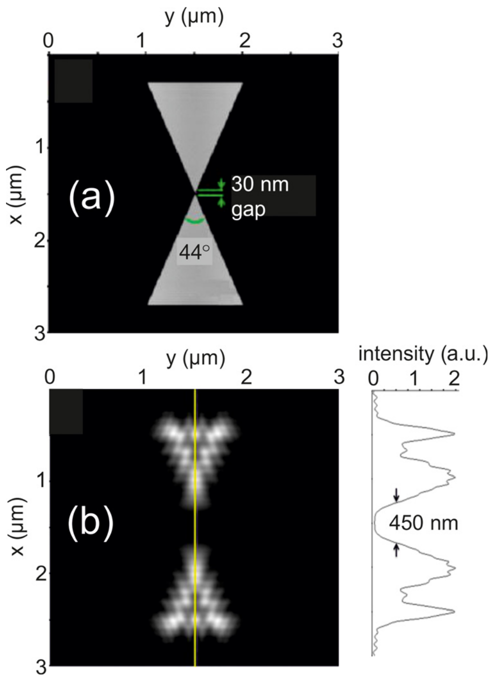

FIG. 7. (Color online) (a) Scheme of the simulated bowtie mask, and the (b) x–y plane intensity image with a 5 μm gap.

electrodes of the bowtie. As an example, the modified bowtie mask was simulated with the aim to reduce the distance between electrodes in the bowtie structure at the same proximity gap of 5 μm. The modified bowtie element in the mask is designed with overlapping electrodes and the opening angle of the triangle is increased to 90° [Fig. 8(a)]. As can be seen from the simulation result in Fig. 8(b), the obtained distance between bowtie electrodes is significantly reduced.

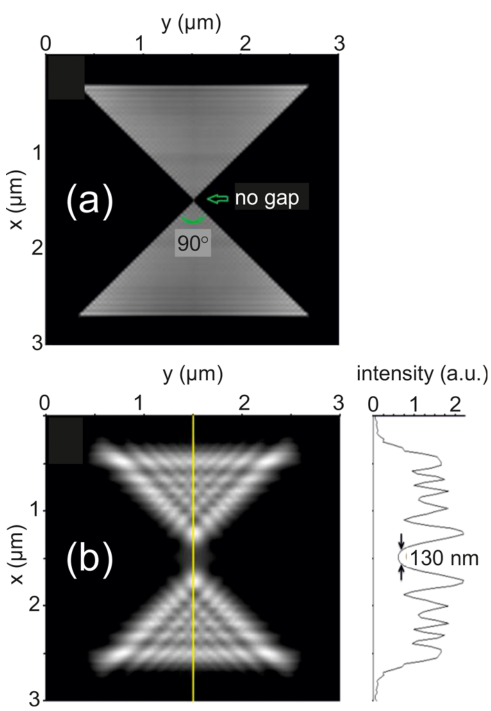

FIG. 8. (Color online) (a) Scheme of the modified bowtie mask, and the (b) aerial image with a 5 μm proximity gap.

The cross-section intensity distribution in Fig. 8(b) at the 5 μm proximity gap shows that the achievable distance between electrodes can be reduced by more than a factor of 3–130 nm while maintaining the same proximity gap and exposure dose; however, additional diffraction minima appear within the triangles. These added minima decrease the required process latitude considerably, elevating the requirements on resist contrast and exposure dose control. Further mask design optimization will be necessary to obtain a larger process window for these bowtie structures and to reduce the distance between bowtie electrodes to the sub-100 nm range.

It is also worth noting that such no-gap transmission are simple to manufacture since reliable production of bowtie arrays with sub-50 nm distance between electrodes is a challenging task even for EBL.

In the future, this work will be extended by including a simulation of the transfer of the aerial image into resists. Moreover, full three-dimensional masks will be rigorously simulated to obtain even more accurate results in close proximity to the mask.

It should be noted that the proposed method does not target the leading edge integrated circuit manufacturing and investigates the diffraction on masks with nanophotonic structures with sizes of the order of half of the application wavelength (typically in visible/IR range). The choice of manufacturing methods for such structure arrays is limited. Besides the low throughput e-beam lithography and cost intensive large scale EUV lithography, the sufficient control over the gap size can be achieved utilizing either directed self-assembly (DSA) or nanoimprint lithography. The relatively large size of single antennae and their complex geometry are making utilization of DSA inefficient. The nanoimprint lithography can be used for creation of such structures.[37,38] As an already established method, it can demonstrate higher throughput, but it is limited with 1:1 replication of structures on the mask and has to deal with issues of mask degradation and contamination due to necessity of contact. The suggested EUV proximity lithography is contact free and allows for additional complexity of the resulting patterns, since the diffraction of EUV radiation on these relatively large structures is governed by Fresnel diffraction laws.

V. SUMMARY AND CONCLUSIONS

In summary, a laboratory-scale setup for EUV proximity lithography has demonstrated the ability to create complex nanoantenna arrays and can be used for cost-effective small- and medium-scale manufacturing of nanophotonic structures. Utilizing a compact partially coherent DPP EUV source and state-of-the-art positioning systems, a knife-edge resolution of 28 nm was achieved. Precise control over the mask-to-wafer gap increases the flexibility of diffraction-assisted EUV lithography, providing the possibility to produce different nanostructures without changing the design of the mask. The established scalar diffraction simulations allowed us to not only predict the experimental results, but also to open a way for implementation of optical proximity correction and increase the quality of structuring and the applicability of the method.

ACKNOWLEDGMENTS

This work was enabled by cooperation activities in the framework of the Jülich Aachen Research Alliance for Fundamentals of Future Information Technology (JARA-FIT). T.T. was financially supported by the Excellence Initiative of the German federal state governments and the Ministry of Innovation of North-Rhine-Westphalia. The authors would also like to acknowledge the excellent cleanroom staff at the Forschungszentrum Jülich for their helpful assistance during the work.

[1]H. I. Smith, Phys. Scr., T **61**, 26 (1996).
[2]A. Heuberger, J. Vac. Sci. Technol. B **6**, 107 (1988).
[3]F. Cerrina, *X-Ray Lithography*, edited by P. Rai-Choudhury (SPIE Press, Bellingham, Washington, 1997).
[4]F. Cerrina, Jpn. J. Appl. Phys. **31**, 4178 (1992).
[5]J. Z. Y. Guo, and F. Cerrina, IBM J. Res. Dev. **37**, 331 (1993).
[6]Y. Vladimirsky, A. J. Bourdillon, O. Vladimirsky, W. Jiang, and Q. Leonard, J. Phys. D: Appl. Phys. **32**, L114 (1999).
[7]A. J. Bourdillon, C. B. Boothroyd, G. P. Williams, and Y. Vladimirsky, J. Phys. D: Appl. Phys. **36**, 2471 (2003).
[8]A. J. Bourdillon and C. B. Boothroyd, J. Phys. D: Appl. Phys. **38**, 2947 (2005).
[9]D. T. Attwood, *Soft X-Rays and Extreme Ultraviolet Radiation* (Cambridge University Press, Cambridge, UK, 2000), p. 408.
[10]K. B. Crozier, A. Sundaramurthy, G. S. Kino, and C. F. Quate, J. Appl. Phys. **94**, 4632 (2003).
[11]P. Mühlschlegel, H.-J. Eisler, O. J. F. Martin, B. Hecht, and D. W. Pohl, Science **308**, 1607 (2005).
[12]L. Novotny, and N. van Hulst, Nat. Photon. **5**, 83 (2011).
[13]P. L. Stiles, J. Dieringer, N. C. Shah, and R. P. Van Duyne, Annu. Rev. Anal. Chem. **1**, 601 (2008).
[14]T. R. Jensen, R. P. Van Duyne, S. A. Johnson, and V. A. Maroni, Appl. Spectrosc. **54**, 371 (2000).
[15]F. Neubrech, A. Pucci, T. Cornelius, S. Karim, A. García-Etxarri, and J. Aizpurua, Phys. Rev. Lett. **101**, 157403 (2008).
[16]R. Adato, P. Natl. Acad. Sci. U.S.A. **106**, 19227 (2009).
[17]E. Cubukcu, E. A. Kort, K. B. Crozier, and F. Capasso, Appl. Phys. Lett. **89**, 093120 (2006).
[18]A. Sundaramurthy, P. J. Schuck, N. R. Conley, D. P. Fromm, G. S. Kino, and W. E. Moerner, Nano Lett. **6**, 355 (2006).
[19]L. Wang, S. M. Uppuluri, E. X. Jin, and X. Xu, Nano Lett. **6**, 361 (2006).
[20]S. Kim, J. Jin, Y.-J. Kim, I.-Y. Park, Y. Kim, and S.-W. Kim, Nature Lett. **453**, 757 (2008).
[21]P. J. Schuck, D. P. Fromm, A. Sundaramurthy, G. S. Kino, and W. E. Moerner, Phys. Rev. Lett. **94**, 017402 (2005).
[22]J. Pankert *et al. EUV Sources for Lithography*, edited by V. Bakshi (SPIE Press, Bellingham, Washington, 2005).
[23]K. Bergmann, O. Rosier, W. Neff, and R. Lebert, Appl. Opt. **39**, 3833 (2000).
[24]K. Bergmann, S. Danylyuk, and L. Juschkin, J. Appl. Phys. **106**, 073309 (2009).
[25]S. Brose *et al*., Thin Solid Films **520**, 5080 (2012).
[26]See: http://www.dowcorning.com/content/etronics/etronicslitho/etronics_litho_ebeam.asp.
[27]See: http://www.zeon.co.jp/business_e/enterprise/imagelec/imagelec.html.
[28]H. J. Levinson, *Principles of Lithography* (SPIE Press, Bellingham, Washington, 2010), p. 462.
[29]S. V. Danylyuk, R. Ott, G. Panaitov, G. Pickartz, E. Hollmann, S. A. Vitusevich, A. E. Belyaev, and N. Klein, Thin Solid Films **515**, 489 (2006).
[30]B. L. Henke, E. M. Gullikson, and J. C. Davis, Atomic Data Nucl. Data Tables **54**, 181 (1993).
[31]M. Born and E. Wolf, *Principles of Optics* (Cambridge University Press, Cambridge, UK, 2003), p. 515.
[32]B. Meliorisz, J. Micro/Nanolith. MEMS MOEMS **6**, 023006 (2007).
[33]D. S. Burch, Am. J. Phys. **53**, 255 (1985).
[34]J. G. Huang, J. M. Christian, and G. S. McDonald, J. Opt. Soc. Am. A **23**, 2768 (2006).
[35]Y. Sonnefraud, N. Verellen, H. Sobhani, G. A. Vandenbosch, V. V. Moshchalkov, P. Van Dorpe, P. Nordlander, and S. A. Maier, ACS Nano **4**, 1664 (2010).
[36]B. Luk'yanchuk, N. Zheludev, S. Maier, N. J. Halas, P. Nordlander, H. Giessen, and C. T. Chong, Nature Mater. **9**, 707 (2010).
[37]C. M. Bruinink, M. Burresi, M. J. de Boer, F. B. Segerink, H. V. Jansen, E. Berenschot, D. N. Reinhoudt, J. Huskens, and L. Kuipers, Nano Lett. **8**, 2872 (2008).
[38]W. Wu *et al*., Appl. Phys. Lett. **90**, 063107 (2007).